

Nucleation and growth controlled reduced graphene oxide-supported palladium electrocatalysts for methanol oxidation reaction

Jen Chao Ng¹, Chou Yong Tan^{1,2} , Boon Hoong Ong³, Atsunori Matsuda⁴, Wan Jeffrey Basirun⁵, Wai Kian Tan⁴ , Ramesh Singh¹, and Boon Kar Yap⁶

Abstract

In spite of advantages of direct methanol fuel cells, low methanol oxidation reaction and fuel crossover from anode to cathode, there remains a challenge that inhibits it from being commercialized. Active electrocatalysts are in high demand to promote the methanol oxidation reaction. The methanol reached at the anode can be immediately reacted, and thus, less methanol to cross to the cathode. The performance of electrocatalysts can be significantly influenced by varying the concentration of precursor solution. Theoretically, concentrated precursor solution facilitates rapid nucleation and growth; diluted precursor solution causes slow nucleation and growth. Rapid nucleation and slow growth have positive effect on the size of electrocatalysts which plays a significant role in the catalytic performance. Upon the addition of appropriate concentration of graphene oxide, the graphene oxide was reported to have stabilizing effect towards the catalyst nanoparticles. This work synthesized reduced graphene oxide-supported palladium electrocatalysts at different concentrations (0.5, 1.0, 2.0, 3.0 and 4.0 mg mL⁻¹) with fixed volume and mass ratio of reduced graphene oxide to palladium by microwave-assisted reduction method. Results showed that reduced graphene oxide-supported palladium synthesized at a concentration of 1.0 mg mL⁻¹ gave the best methanol oxidation reactivity (405.37 mA mg⁻¹) and largest electrochemical active surface area (83.57 m² g⁻¹).

Keywords

Graphene, palladium nanocatalysts, nucleation and growth control, methanol oxidation reaction, microwave synthesis

Date received: 17 April 2018; accepted: 26 December 2018

Topic: Nanoparticles and Colloids
Topic Editor: Raphael Schneider
Associate Editor: Raphael Schneider

Introduction

Depletion of fossil fuels in near future and its arisen pollution issue have sparked interest of scientists and engineers to seek for alternative energy supply.¹ Direct methanol fuel cells (DMFCs) emerge to be suitable green power source that directly convert chemical energy into electric energy for portable electronic devices owing to its low operating temperature, high theoretical energy density, low-cost liquid fuel and relatively quick start-up.^{2–4} Nonetheless, the methanol at the anode tends to permeate through the

¹ Department of Mechanical Engineering, Faculty of Engineering, University of Malaya, Kuala Lumpur, Malaysia

² School of Mechanics, Civil Engineering and Architecture, Northwestern Polytechnical University, Xi'an, China

³ Nanotechnology and Catalysis Research Centre, University of Malaya, Kuala Lumpur, Malaysia

⁴ Department of Electrical and Electronic Information Engineering, Toyohashi University of Technology, Toyohashi, Aichi, Japan

⁵ Department of Chemistry, Faculty of Science, University of Malaya, Kuala Lumpur, Malaysia

⁶ Department of Electronics and Communication, College of Engineering, Universiti Tenaga Nasional, Kajang, Selangor, Malaysia

Corresponding author:

Chou Yong Tan, Department of Mechanical Engineering, Faculty of Engineering, University of Malaya, Kuala Lumpur 50603, Malaysia; School of Mechanics, Civil Engineering and Architecture, Northwestern Polytechnical University, Xi'an, China.
Email: choyong@um.edu.my



electrolyte membrane into the cathode.⁵ This results in reduced cell voltage (sometimes called a mixed potential), flow of internal currents and a waste of fuel.⁶ A solution to this problem is to synthesize active anodic electrocatalysts. Active electrocatalysts allow the methanol reached at the anode to be reacted effectively. Hence, this will cause less methanol available to diffuse through the electrolyte to the cathode.⁶

Active electrocatalysts can be characterized by large electrochemically active surface area (ECSA), which can be obtained by less agglomerated and small-sized catalysts.⁷ Loading catalysts onto the surface of graphene has been found effective in limiting the aggregation and size of catalysts.^{8,9} Previous works have provided in-depth studies on the unique properties of graphene and its contribution to the performances of graphene-related electrocatalysts.^{10,11} Its large surface area ($2630 \text{ m}^2 \text{ g}^{-1}$) immobilizes catalysts on the surface, making the catalysts stable, smaller and less agglomerated, maximizing catalyst utilization and catalytic sites for reactions.⁵

Formation of nanoparticles (NPs) involves three steps: (i) generation of supersaturation, (ii) nucleation and (iii) growth of NPs.¹² Current research has been focusing on growth controlling by using surfactants such as polyvinylpyrrolidone,¹³ polyvinyl alcohol¹⁴ and poly(diallyldimethylammonium chloride).¹⁵ Nonetheless, there are reports stating that surfactants will cover the active sites of catalysts, thereby limiting the catalytic activity.¹⁵ In fact, the size of catalysts can also be controlled through careful manipulation of the concentration of precursors.¹² The precursors can be reduced by ethylene glycol (EG). During the reduction process, EG reduces the starting precursors to final products and itself gets oxidized to carbonyl compound (mainly diacetyl).^{16,17} Notably, reduction capability of EG is rather weak. Sodium hydroxide (NaOH) is added to accelerate the reduction reaction by inducing monoanion of EG, which has been reported active towards reduction reaction.¹⁸ High concentration favours the rate of the above three steps.¹² Nevertheless, varied to the first two steps, fast growth of NPs is unintended because it leads to the formation of large particle.¹²

To date, the number of work reported on the effect of concentration of precursor mixture (graphene oxide (GO) + metal ions) is scarce. Therefore, the objective of this work is to investigate the effects of various concentrations of starting precursor (palladium chloride (PdCl_2) + GO) on the catalytic activity of the electrocatalysts at a fixed mass ratio of palladium (Pd) to GO.

Experimental

Materials

Graphite flake (50 mesh) was purchased from Asbury Carbons (Asbury, New Jersey, USA). Concentrated phosphoric acid (H_3PO_4) and potassium permanganate (KMnO_4) were

obtained from Wako Pure Chemical Industries, Ltd (Chuo-ku, Osaka, Japan). Concentrated sulphuric acid (H_2SO_4), hydrogen peroxide (H_2O_2), fuming hydrochloric acid (HCl, 37%), PdCl_2 , EG, Nafion, NaOH and potassium hydroxide (KOH) were from Sigma-Aldrich (Meguro-ku, Tokyo, Japan). All chemicals were analytically pure and used as received without further purification. The deionized (DI) water for solution preparation was produced from Advantec Aquarius RFD230NA, Japan (conductivity = $0.06 \mu\text{S}$).

Pd/reduced GO preparation

Graphite flake was oxidized to graphite oxide by improved Hummers' method published elsewhere with slight modification, but the main features are briefly illustrated here.¹⁹ H_2SO_4 was mixed with H_3PO_4 at a ratio of 360:40 mL followed by the addition of 3 g of graphite flake. Then, 18 g of KMnO_4 was added into the above mixture and stirred. After 3 days of stirring, by immersing in ice bath, 500 mL of DI water was added to the above mixture, and 17 mL of H_2O_2 was added dropwise to halt the oxidation. The mixture was then sequentially washed with 1 M of HCl thrice at 6000 r min^{-1} for 30 min, and followed up by using DI water for seven times at $10,000 \text{ r min}^{-1}$ for 1 h by centrifugation. Next, the synthesized graphite oxide was dried overnight at 60°C in an oven.

For the synthesis of reduced graphene oxide (rGO)-supported Pd (Pd/rGO) at concentration 0.5 mg mL^{-1} , denoted as Pd/rGO (0.5), the dried graphite oxide (30 mg) was dispersed in 80 mL of DI water and ultrasonicated for 2 h to obtain GO. Subsequently, 50 mg of PdCl_2 was added and sonicated for 30 min. Then, the above mixture was stirred for 1 h at room temperature. Meanwhile, 80 mL of EG was added dropwise. The pH of the mixture was adjusted to 10 by 1 M of NaOH. Subsequently, the mixture was reduced by household microwave oven at 700 W for 700 s. Finally, the resulting black solid powders were washed by DI water thrice via centrifugation at 6000 r min^{-1} for 30 min and were dried overnight in an oven at 60°C . The samples with other concentrations (1.0, 2.0, 3.0 and 4.0 mg mL^{-1} , denoted as Pd/rGO (1.0), Pd/rGO (2.0), Pd/rGO (3.0) and Pd/rGO (4.0), respectively) as recorded in Table 1 were synthesized by repeating the above procedures with different mass of GO and Pd.

Characterization

The characterization of morphologies and compositions of the samples were performed by field-emission scanning electron microscopy (FESEM; HITACHI S-4800, Chiyoda-ku, Tokyo, Japan) coupled with energy dispersive X-ray spectroscopy (EDX). Raman analysis, a non-destructive characterization technique, was used to investigate the defect levels, crystallinity and structure. The procedure was performed by a JASCO NRS-3100 (Easton,

Table I. Samples of different total mass of GO and PdCl₂ mixture, and concentration.

Electrocatalysts	Mass of GO (mg)	Mass of PdCl ₂ (mg)	Volume of mixture solution (mL)	Concentration of mixture solution (mg mL ⁻¹)
Pd/rGO (0.5)	30	50	160	0.5
Pd/rGO (1.0)	60	100	160	1.0
Pd/rGO (2.0)	120	200	160	2.0
Pd/rGO (3.0)	180	300	160	3.0
Pd/rGO (4.0)	240	400	160	4.0

PdCl₂: palladium chloride; Pd: palladium; GO: graphene oxide; rGO: reduced graphene oxide; Pd/rGO: reduced graphene oxide-supported palladium.

Maryland, USA) equipped with a charge-coupled-device detector using Argon ion at a wavelength of 532 nm. The crystallite structures were investigated by X-ray powder diffraction (XRD) by using an Ultima IV X-ray diffractometer (Rigaku, [Matsubara-cho, Akishima-shi, Tokyo, Japan], USA) with a Cu X-ray source ($\lambda = 0.1541$ nm) operating at 40 kV and 40 mA. Fourier-transform infrared (FTIR) spectroscopy (Shimadzu TCC-240A, Nakagyo-ku, Kyoto, Japan) was conducted to verify the successful reduction of the samples.

Electrochemical measurement

All the electrochemical experiments were examined with a conventional three-electrode electrochemical cell by using a Solartron 1280C (Farnborough, Hampshire, UK) with computerized control by ZPlot software at room temperature. A platinum sheet of 1 cm², silver/silver chloride (Ag/AgCl) (3 M potassium chloride (KCl)) electrode and glassy carbon electrode (GCE; 3.0 mm diameter) were used as counter, reference and working electrodes, respectively.

To prepare the working electrode, 2 mg as-prepared catalysts were first dispersed in 1 mL DI water and ultrasonicated for 30 min. Then, 10 μ L of the suspension was casted onto the surface of polished GCE and dried in an oven at 60°C. Subsequently, 5 μ L of Nafion (0.05 wt%) was dropped onto the electrode surface and dried at 60°C in the oven.

The ECSA of each electrocatalyst was conducted by cyclic voltammetry (CV) measurement in a solution of 1 M KOH from -1.0 V to 0.6 V versus Ag/AgCl. Meanwhile, methanol oxidation activity was investigated by CV measurements in 1 M KOH + 1 M methanol at similar potential range. All the electrochemical tests were carried out at a scan rate of 50 mV s⁻¹ for 10 runs. Chronoamperometry (CA) measurements were studied in the same methanol-contained KOH solution at an applied voltage of -0.2 V for 1000 s. Electrolytes were all purged with nitrogen gas for 30 min to remove any dissolved oxygen prior to the measurements.

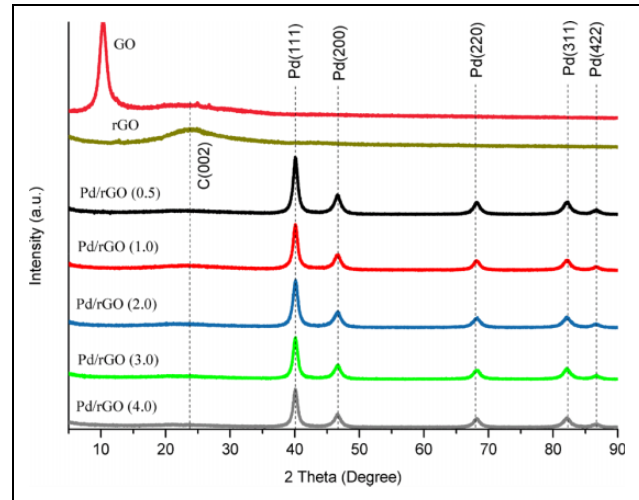


Figure 1. XRD images of Pd/rGO (0.5), Pd/rGO (1.0), Pd/rGO (2.0), Pd/rGO (3.0) Pd/rGO (4.0), rGO and GO. XRD: X-ray powder diffraction; Pd: palladium; GO: graphene oxide; rGO: reduced graphene oxide; Pd/rGO: reduced graphene oxide-supported palladium.

Results and discussion

Characterization

Crystalline phase structures of samples were characterized by XRD measurement. Figure 1 shows the XRD of GO, rGO and Pd/rGO at different concentrations. The disappearance of the peak of GO at 10.3°, and appearance of weak and broad peak at 24°, which belongs to C(002) planes of rGO, imply that GO sheets were successfully reduced by microwave irradiation for all samples.²⁰ Meanwhile, the peaks at approximately 40.1°, 46.5°, 68.2°, 82.1° and 86.69° could be indexed to the (111), (200), (220), (311) and (422) lattice planes of the face-centred cubic crystalline structure of Pd (JCPDS No. 46-1043), respectively. By using Scherrer's formula based on the Pd (220) peak, the particle size of Pd was calculated to be 8.69, 8.08, 7.57, 8.32 and 8.64 nm for Pd/rGO (0.5), Pd/rGO (1.0), Pd/rGO (2.0), Pd/rGO (3.0) and Pd/rGO (4.0), respectively. Increasing the concentration to 1.0 mg mL⁻¹, the particle size became smaller. Such phenomenon can be rationalized by Figure 2. The nucleus formed is stable only when it overcomes the critical energy (ΔG^*) and exceeds the critical size (r^*). Equations (1) to (5) are the related formulas¹²

$$\Delta G^* = \frac{16\pi\gamma}{(3\Delta G_v)^2} \quad (1)$$

$$\Delta G_v = -\frac{kT}{\Omega} \ln\left(\frac{C}{C_0}\right) \quad (2)$$

$$\Delta G_v = -\frac{kT}{\Omega} \ln(1 + O') \quad (3)$$

$$O' = C - C_0/C_0 \quad (4)$$

$$r^* = \frac{-2\gamma}{\Delta G_v} \quad (5)$$

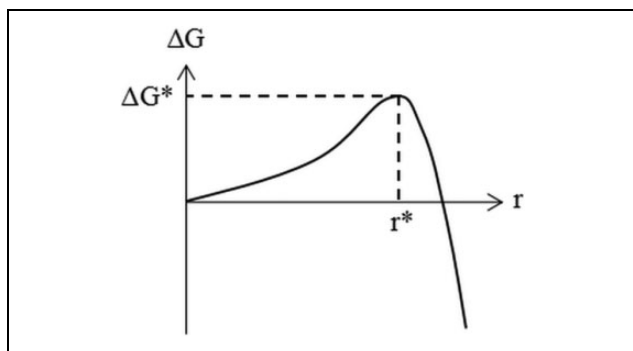


Figure 2. Figure illustrating the change of total free energy, ΔG , as function of nucleus' radius, r .

where γ is the surface energy per unit area of the formed nucleus, ΔG_v is the change of Gibbs free energy per unit volume of the nucleus, C is the concentration of the solute, C_o is the equilibrium concentration or solubility, k is the Boltzmann constant, T is the temperature and O' is the supersaturation. From the above equations, the critical size and critical energy can be reduced with increased supersaturation that relates to concentration. High initial concentration favours the formation of a large number of nuclei, signifying smaller sized nuclei.¹² Nevertheless, further increment of concentration beyond 1.0 mg mL^{-1} resulted in bigger Pd NPs. At concentration beyond 1.0 mg mL^{-1} , the newly formed small nuclei have high surface energy, causing it to be unstable. Thus, the small nuclei tend to grow bigger by Ostwald ripening and agglomeration to reduce the surface energy.¹² At concentration beyond 1.0 mg mL^{-1} , nuclei are in close proximity, and collide with each other all the time, resulting in large agglomeration and high growth rate.¹²

Figure 3(a) to (e) shows transmission electron microscopy (TEM) images of the Pd/rGOs at different concentrations. Mean particle size as well as size distribution were calculated from 50 NPs and are shown in Figure 3(f) to (j). Wrinkles and ripples that induced from the removal of oxygen-containing functional groups of GO can clearly be observed for all samples.²¹ Pd NPs appeared as dark dots on the transparent rGO sheets. The Pd NPs were successfully loaded onto the surface of the rGO for all samples. Serious agglomeration with wide size distribution occurred at Pd/rGO (0.5) because the low concentration of GO was unable to stabilize the Pd NPs. At concentration 1.0 mg mL^{-1} , the agglomeration was alleviated. The GO is at appropriate concentration to stabilize the Pd NPs, uniformly distributing the Pd NPs on rGO surface and contributing to narrow size distribution. Further increment in concentration beyond 1.0 mg mL^{-1} resulted in wide particle size range and serious agglomeration because of the close proximity between neighbouring particles. The particles agglomerated together to reduce surface energy. The tendency of agglomeration of NPs exceeded the stabilizing effect of GO for concentrated precursor mixture with

concentration beyond 1.0 mg mL^{-1} . The Pd NPs of Pd/rGO (1.0) were further observed at higher resolution (Figure 3(k)). The high-resolution TEM image revealed a lattice spacing of 0.22 nm , corresponding to the Pd (111) crystal-line planes.

EDX (Table 2) shows higher mass loading of Pd for more concentrated samples with the Pd/rGO (2.0) having the highest amount of Pd deposition. Correlating to the FESEM images, it suggests that the high mass loading leads to agglomeration. The unexpected lower mass of Pd/rGO (3.0) and Pd/rGO (4.0) could be explained by the possible severe agglomeration that detach from rGO surface during centrifugation.

Raman characterization was performed to analyse the defect level and quality of rGO.²² As shown in Figure 4, all samples present two intense peaks at $1330\text{--}1350 \text{ cm}^{-1}$ and approximately 1590 cm^{-1} that correspond to D band and G band, respectively. The former peak was attributed to the structural disorder or intrinsic defects due to an A_{1g} vibrational mode. The latter was related to the first-order scattering of the E_{2g} mode of graphite that was associated to the coplanar vibration of sp^2 -hybridized carbon atoms in a two-dimensional hexagonal lattice.²³ The intensity ratio of D band to G band (I_D/I_G) is an indicator of degree of disorder in graphitic structure.²¹ Compared to GO ($I_D/I_G = 1.00$), all samples displayed increased ratio as recorded in Figure 4, signalling successful reduction of GO and loading of Pd NPs on rGO.^{24,25} Increased D band suggested more sp^2 domains with smaller size were generated upon reduction of GO.²³ The chemical reduction induced defects, such as edges and ripples, to the graphitic plane.²¹ Interaction of metal NPs with rGO also created superficial defects to the rGO, thereby Pd/rGO (2.0), Pd/rGO (3.0) and Pd/rGO (4.0) with high Pd mass loading reported high value of I_D/I_G .²⁶ Appropriate level of defects has been reported to promote Pd dispersion with high uniformity.²⁷ This explains for the better distribution of Pd/rGO (1.0). Notably, the unique properties of graphene would be destructed when the defects are high.^{7,23} The defects serve as nucleation centres for clustering where the Pd NPs migrate over the rGO and coalesce at its vicinity.²⁶ This can be another factor of the agglomeration of the samples with concentration beyond 1.0 mg mL^{-1} .

Figure 5 shows FTIR spectra of the GO and samples at different concentrations. All samples exhibited rather similar spectra. Peaks of GO can clearly be observed at 1126 , 1637 and 3431 cm^{-1} , corresponding to C–O stretching vibration, sp^2 -hybridized C=C stretching vibrations and OH stretching vibration, respectively.²⁸ Most of the associated oxygen-containing peaks were removed or greatly decreased after the reduction process, verifying the successful reduction of the samples despite some weak residual O–H peaks can be observed at approximately 1048 and 1173 cm^{-1} .²⁹ Some new peaks also appeared at approximately 2923 and 2852 cm^{-1} , attributed to the

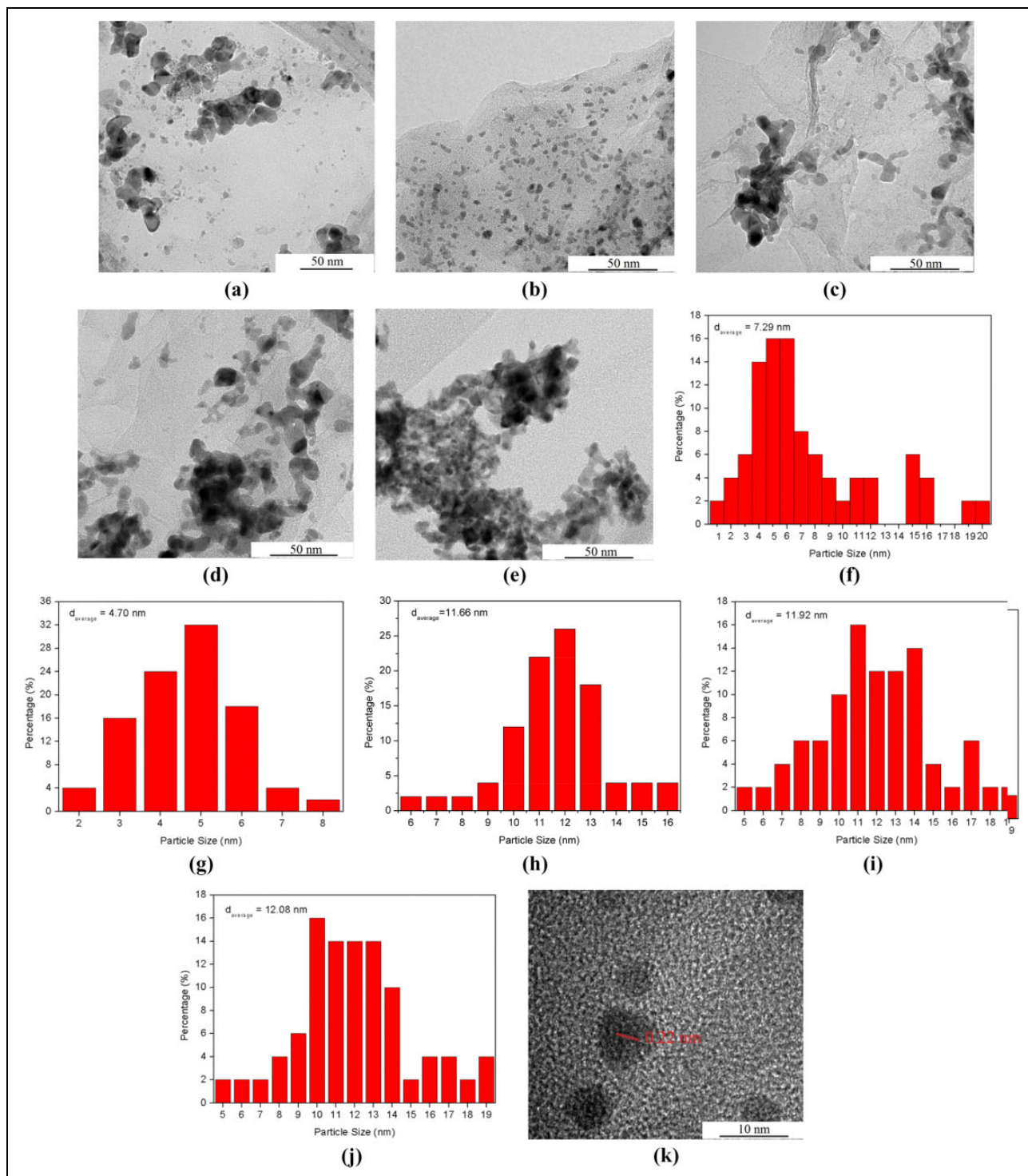


Figure 3. TEM images of (a) Pd/rGO (0.5), (b) Pd/rGO (1.0), (c) Pd/rGO (2.0), (d) Pd/rGO (3.0) and (e) Pd/rGO (4.0). NP size distribution of (f) Pd/rGO (0.5), (g) Pd/rGO (1.0), (h) Pd/rGO (2.0), (i) Pd/rGO (3.0) and (j) Pd/rGO (4.0). (k) HRTEM image of Pd/rGO (1.0). TEM: transmission electron microscopy; Pd: palladium; rGO: reduced graphene oxide; Pd/rGO: reduced graphene oxide-supported palladium; HRTEM: high-resolution transmission electron microscopy; NP: nanoparticle.

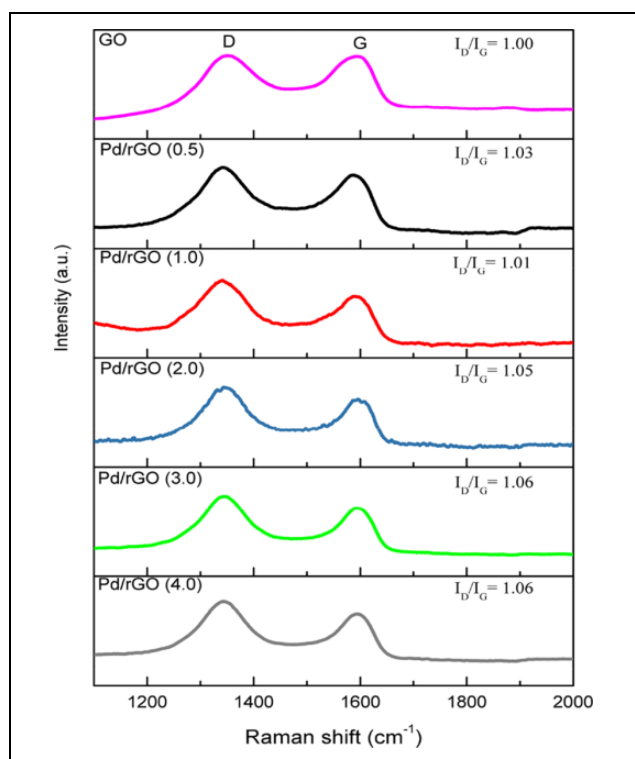
CH₂ stretching vibration and CH stretching vibrations, respectively.³⁰ The appearance of these new peaks can be ascribed to the reduction of the carboxylic acids in GO to

CH₂OH. The strong peak at 1575 cm⁻¹, associating to skeletal vibration of sp²-hybridized carbon ring in graphene, suggested the recovery of sp² lattice.²⁹

Table 2. The EDX of Pd/rGO (0.5), Pd/rGO (1.0), Pd/rGO (2.0), Pd/rGO (3.0) and Pd/rGO (4.0).

Electrocatalysts	Weight percentage, wt%		
	Pd	C	O
Pd/rGO (0.5)	53.42	32.01	14.57
Pd/rGO (1.0)	53.37	31.95	12.68
Pd/rGO (2.0)	73.29	20.00	6.72
Pd/rGO (3.0)	69.03	23.39	7.58
Pd/rGO (4.0)	69.27	24.22	6.51

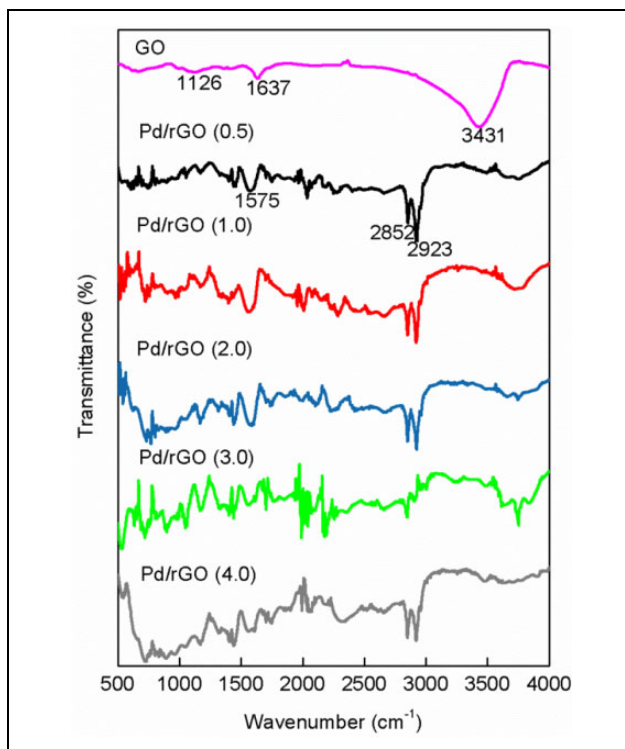
EDX: energy dispersive X-ray spectroscopy; Pd: palladium; rGO: reduced graphene oxide; Pd/rGO: reduced graphene oxide-supported palladium.

**Figure 4.** Raman images of Pd/rGO (0.5), Pd/rGO (1.0), Pd/rGO (2.0), Pd/rGO (3.0), Pd/rGO (4.0) and GO. Pd: palladium; GO: graphene oxide; rGO: reduced graphene oxide; Pd/rGO: reduced graphene oxide-supported palladium.

Electrochemical measurements

The ECSA of the electrocatalysts accounts for the number of catalytic sites that are active for electrochemical reaction and provides information on the conductive path accessible for electron transfer to and from the electrode surface.^{5,31} The values of ECSA were calculated from the area of reduction peak of palladium oxide (PdO) in the potential region of -0.7 to -0.2 V versus Ag/AgCl on the CV in Figure 6(a) according to Equation (6)³²

$$\text{ECSA} = \frac{Q}{Sl} \quad (6)$$

**Figure 5.** FTIR spectra of GO, Pd/rGO (0.5), Pd/rGO (1.0), Pd/rGO (2.0), Pd/rGO (3.0) and Pd/rGO (4.0). FTIR: Fourier-transform infrared; Pd: palladium; GO: graphene oxide; rGO: reduced graphene oxide; Pd/rGO: reduced graphene oxide-supported palladium.

where ‘ Q ’ is the coulombic charge (mC) for the PdO reduction, ‘ S ’ is a conversion factor corresponding to 0.424 mC cm^{-2} and ‘ l ’ is the mass of catalyst (mg) loaded on the GCE.³² Table 3 reports the ECSA values of various electrocatalysts ranging from $30.68 \text{ m}^2 \text{ g}^{-1}$ to $83.57 \text{ m}^2 \text{ g}^{-1}$. Well distribution of Pd NPs on the surface of rGO, small particle size (8.08 nm) and less defects of rGO (as reflected by $\frac{I_D}{I_G} = 1.01$) render Pd/rGO (1.0) highest ECSA.

The electro-oxidation of methanol of as-prepared electrocatalysts is shown in Figure 6(b). Relating to the XRD result, where Pd (111) crystal facets predominate for all samples, it can be inferred that Pd (111) is mainly responsible for the methanol oxidation reaction (MOR). Two peaks, which are forward peak at approximately -0.1 V and reverse peak at approximately -0.4 V, can be observed. The forward peak can be attributed to the methanol oxidation and the reverse peak can be ascribed by the oxidation of the residual carbon species.³³ Peak current density and peak potential of electrocatalysts are recorded in Table 3. The highest current density of Pd/rGO (1.0) can be attributed to the small size, uniform distribution and large ECSA of Pd catalysts. CA in Figure 6(c) reveals that Pd/rGO (1.0) retained highest current density and smallest current drop (Table 3). The better stability can be ascribed to the lower defect level because defects cause the as-synthesized electrocatalysts to corrode easily under

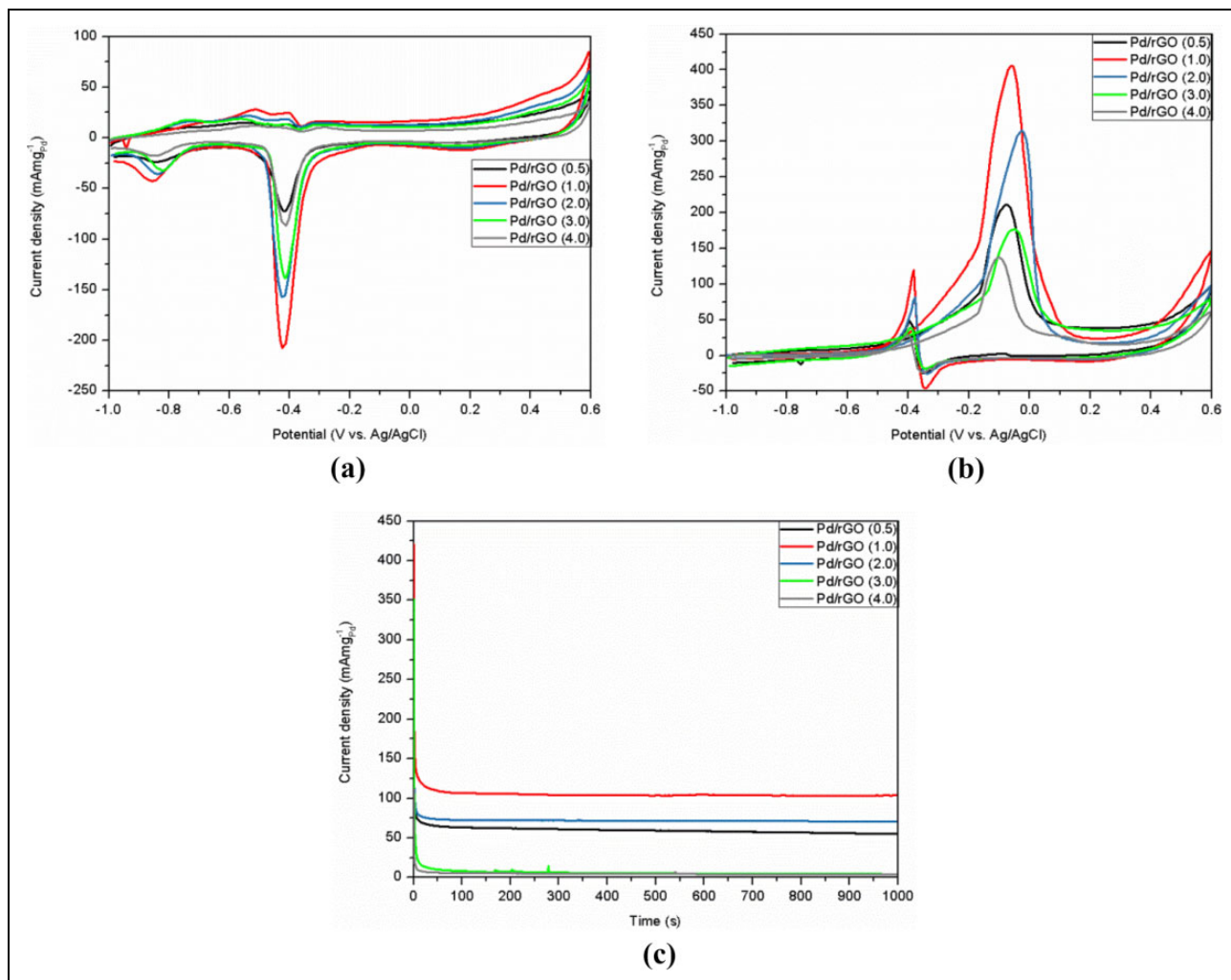


Figure 6. The cyclic voltammograms of Pd/rGO (0.5), Pd/rGO (1.0), Pd/rGO (2.0), Pd/rGO (3.0) and Pd/rGO (4.0) in nitrogen saturated solutions of (a) 1 M KOH and (b) 1 M KOH/1 M CH₃OH with scan rate of 50 mV s⁻¹. (c) The chronoamperogram of Pd/rGO (0.5), Pd/rGO (1.0), Pd/rGO (2.0), Pd/rGO (3.0) and Pd/rGO (4.0) in nitrogen saturated solution of 1 M KOH/1 M CH₃OH with scan rate of 50 mV s⁻¹ at an applied potential of -0.2 V. Pd: palladium; rGO: reduced graphene oxide; Pd/rGO: reduced graphene oxide-supported palladium; KOH: potassium hydroxide; CH₃OH: methanol.

Table 3. ECSA, peak potential, peak current density and percentage of current drop over time of various Pd/rGOs.

Catalyst	ECSA (m ² g ⁻¹)	Peak potential (V vs. Ag/AgCl)	Peak current density (mA mg ⁻¹ _{Pd})	Percentage of current drop over time (%)
Pd/rGO (0.5)	30.68	-0.074	212.22	9.89
Pd/rGO (1.0)	83.57	-0.062	405.37	1.22
Pd/rGO (2.0)	63.80	-0.026	314.36	2.21
Pd/rGO (3.0)	45.78	-0.053	177.25	32.74
Pd/rGO (4.0)	33.37	-0.104	137.59	22.22

ECSA: electrochemically active surface area; AgCl: silver chloride; Ag: silver; Pd: palladium; rGO: reduced graphene oxide; Pd/rGO: reduced graphene oxide-supported palladium.

electrochemical operation.²³ Owing to the attachment of intermediate species that were generated during methanol electro-oxidation to the surface of electrocatalysts, initial

current density dropped rapidly.³⁴ When the poisoning species released over time, approximately 100 s, the current dropped steadily.³⁵

Conclusions

By keeping the ratio of Pd to rGO fixed at 1:1, Pd/rGOs of different concentrations were successfully synthesized by microwave reduction method in EG solution. Altering the concentration, the rate of nucleation and growth of NPs and stabilizing effect of GO change. These changes manipulate the mean particle size and distribution of catalysts on the surface of rGO. At concentration 0.5 mg mL^{-1} , the GO was unable to stabilize the Pd NPs, furthermore, the rate of nucleation is low, forming large nuclei. By contrary, concentration at 1.0 mg mL^{-1} and beyond favoured the nucleation of large number of nuclei, meaning small-sized nuclei. However, concentration beyond 1.0 mg mL^{-1} resulted in rapid growth, leading to large particle size. The NPs were at close proximity in mixture with concentration beyond 1.0 mg mL^{-1} , causing them to agglomerate together to reduce surface energy, and even overwhelmed the stabilizing capability of GO. Altering the concentration, the difference in NP size and MOR is approximately 15% and 195%, respectively. Results proved that 1.0 mg mL^{-1} is the optimum concentration.

Authors' note

Chou Yong Tan and Boon Kar Yapa are also affiliated with International School of Advanced Materials, School of Materials Science and Engineering, South China University of Technology, 510640 Guangzhou, China. The raw/processed data required to reproduce these findings cannot be shared at this time as the data also form part of an ongoing study.

Declaration of conflicting interests

The author(s) declared no potential conflicts of interest with respect to the research, authorship and/or publication of this article.

Funding

The author(s) disclosed receipt of the following financial support for the research, authorship and/or publication of this article: This study was supported under the Frontier Research Grant (grant no. FG0011-17AFR), Postgraduate Research Grant (PPP; grant no. PG207-2015A) and Nippon Sheet Glass Foundation for Materials Science and Engineering (NSG Foundation; research grant no. IF014-2017). The authors gratefully acknowledge AUN/SEED-Net, JICA, University of Malaya and the Ministry of Higher Education Malaysia for the financial support.

ORCID iD

Chou Yong Tan  <https://orcid.org/0000-0001-7970-9714>
Wai Kian Tan  <https://orcid.org/0000-0002-0014-5475>

References

- Salvi BL, Subramanian KA and Panwar NL. Alternative fuels for transportation vehicles: a technical review. *Renew Sustain Energ Rev* 2013; 25: 404–419.
- Zhang Y, Chang G, Shu H, et al. Synthesis of Pt–Pd bimetallic nanoparticles anchored on graphene for highly active

- methanol electro-oxidation. *J Power Sources* 2014; 262: 279–285.
- Chen M, Meng Y, Zhou J, et al. Platinum nanoworms self-assemble on β -cyclodextrin polymer inclusion complexes functionalized reduced graphene oxide as enhanced catalyst for direct methanol fuel cells. *J Power Sources* 2014; 265: 110–117.
- Ojani R, Raof JB, Goli M, et al. Pt–Co nanostructures electrodeposited on graphene nanosheets for methanol electrooxidation. *J Power Sources* 2014; 264: 76–82.
- Zheng JN, Li SS, Chen FY, et al. Facile synthesis of platinum–ruthenium nanodendrites supported on reduced graphene oxide with enhanced electrocatalytic properties. *J Power Sources* 2014; 266: 259–267.
- Larminie J and Dicks A. *Fuel cell systems explained*. 2nd ed. England: Wiley, 2003, p. 466.
- Ensafi AA, Jafari-Asl M and Rezaei B. A new strategy for the synthesis of 3-D Pt nanoparticles on reduced graphene oxide through surface functionalization, Application for methanol oxidation and oxygen reduction. *Electrochim Acta* 2014; 130: 397–405.
- Li L, Chen M, Huang G, et al. A green method to prepare Pd–Ag nanoparticles supported on reduced graphene oxide and their electrochemical catalysis of methanol and ethanol oxidation. *J Power Sources* 2014; 263: 13–21.
- Singh G, Choudhary A, Haranath D, et al. ZnO decorated luminescent graphene as a potential gas sensor at room temperature. *Carbon* 2012; 50: 385–394.
- Chen D, Tang L and Li J. Graphene-based materials in electrochemistry. *Chem Soc Rev* 2010; 39: 3157–3180.
- Shih CJ, Wang QH, Jin Z, et al. Disorder imposed limits of mono- and bilayer graphene electronic modification using covalent chemistry. *Nano Lett* 2013; 13: 809–817.
- Cao G. *Nanostructures and nanomaterials: synthesis, properties and applications*. 1st ed. London: Imperial College Press, 2004.
- Lv JJ, Li SS, Wang AJ, et al. One-pot synthesis of monodisperse palladium–copper nanocrystals supported on reduced graphene oxide nanosheets with improved catalytic activity and methanol tolerance for oxygen reduction reaction. *J Power Sources* 2014; 269: 104–110.
- Su Y, Jiang H, Zhu Y, et al. Hierarchical porous iron and nitrogen co-doped carbons as efficient oxygen reduction electrocatalysts in neutral media. *J Power Sources* 2014; 265: 246–253.
- Yang S, Qiu P and Yang G. Graphene induced formation of single crystal Pt nanosheets through 2-dimensional aggregation and sintering of nanoparticles in molten salt medium. *Carbon* 2014; 77: 1123–1131.
- Bonet F, Tekaiia-Elhsissen K and Sarathy KV. Study of interaction of ethylene glycol/PVP phase on noble metal powders prepared by polyol process. *B Mater Sci* 2000; 23: 165–168.
- Samiee L, Dehghani Mobarake M, Karami R, et al. Developing of ethylene glycol as a new reducing agent for preparation of Pd–Ag/PSS composite membrane for hydrogen separation. *J Petrol Sci Eng* 2012; 2: 25–32.

18. Matsumoto T, Takahashi K, Kitagishi K, et al. Dissolution and reduction of cobalt ions in the polyol process using ethylene glycol: identification of the active species and its role. *New J Chem* 2015; 39: 5008–5018.
19. Chen J, Yao B, Li C, et al. An improved Hummers method for eco-friendly synthesis of graphene oxide. *Carbon* 2013; 64: 225–229.
20. Monteverde Videla AHA, Ban S, Specchia S, et al. Non-noble Fe–NX electrocatalysts supported on the reduced graphene oxide for oxygen reduction reaction. *Carbon* 2014; 76: 386–400.
21. Antony RP, Preethi LK, Gupta B, et al. Efficient electrocatalytic performance of thermally exfoliated reduced graphene oxide–Pt hybrid. *Mater Res Bull* 2015; 70: 60–67.
22. Esmacili A and Entezari MH. Facile and fast synthesis of graphene oxide nanosheets via bath ultrasonic irradiation. *J Colloid Interf Sci* 2014; 432: 19–25.
23. Zhao J, Li H, Liu Z, et al. An advanced electrocatalyst with exceptional electrocatalytic activity via ultrafine Pt-based trimetallic nanoparticles on pristine graphene. *Carbon* 2015; 87: 116–127.
24. Ji Z, Shen X, Xu Y, et al. Anchoring noble metal nanoparticles on CeO₂ modified reduced graphene oxide nanosheets and their enhanced catalytic properties. *J Colloid Interf Sci* 2014; 432: 57–64.
25. Chen DJ, Zhang QL, Feng JX, et al. One-pot wet-chemical co-reduction synthesis of bimetallic gold–platinum nanochains supported on reduced graphene oxide with enhanced electrocatalytic activity. *J Power Sources* 2015; 287: 363–369.
26. Martins CA, Fernández PS, de Lima F, et al. Remarkable electrochemical stability of one-step synthesized Pd nanoparticles supported on graphene and multi-walled carbon nanotubes. *Nano Energy* 2014; 9: 142–151.
27. Du HY, Wang CH, Hsu HC, et al. Graphene nanosheet–CNT hybrid nanostructure electrode for a proton exchange membrane fuel cell. *Int J Hydrogen Energ* 2012; 37: 18989–18995.
28. Zhang M, Li Y, Yan Z, et al. Improved catalytic activity of cobalt core platinum shell nanoparticles supported on surface functionalized graphene for methanol electro-oxidation. *Electrochim Acta*. 2015; 158: 81–88.
29. Andrijanto E, Shoelarta S, Subiyanto G, et al. Facile synthesis of graphene from graphite using ascorbic acid as reducing agent. In: Sutikno Khairurrijal, Susanto H, Suryana R, Triyana K and Markusdiantoro (eds) *AIP conference proceedings*. Grasia Hotel, Semanang City, Indonesia, Melville, New York USA: AIP Publishing, 6–7 October 2015, pp. 020003-1–020003-4.
30. Basirun WJ, Sookhakian M, Baradaran S, et al. Solid-phase electrochemical reduction of graphene oxide films in alkaline solution. *Nanoscale Res Lett* 2013; 8: 397.
31. Hsieh CT, Gu JL, Chen YC, et al. Pulse microwave synthesis of palladium catalysts on graphene electrodes for proton exchange membrane fuel cells. *Electrochim Acta* 2013; 98: 39–47.
32. Qi J, Benipal N, Liang C, et al. PdAg/CNT catalyzed alcohol oxidation reaction for high-performance anion exchange membrane direct alcohol fuel cell (alcohol = methanol, ethanol, ethylene glycol and glycerol). *Appl Catal B Environ* 2016; 199: 494–503.
33. Feng H, Liu Y and Li J. Highly reduced graphene oxide supported Pt nanocomposites as highly efficient catalysts for methanol oxidation. *Chem Commun* 2015; 51: 2418–2420.
34. Ma Ca, Liu W, Shi M, et al. Low loading platinum nanoparticles on reduced graphene oxide-supported tungsten carbide crystallites as a highly active electrocatalyst for methanol oxidation. *Electrochim Acta* 2013; 114: 133–141.
35. Kakaei K and Dorraji M. One-pot synthesis of Palladium Silver nanoparticles decorated reduced graphene oxide and their application for ethanol oxidation in alkaline media. *Electrochim Acta* 2014; 143: 207–215.